Les Cahiers du GERAD ISSN: 0711–2440

A simulation framework for network performance evaluation of large-scale RF-mesh AMIs

F. Malandra
B. Sansò

G–2016–19

March 2016
Revised: April 2017

La collection *Les Cahiers du GERAD* est constituée des travaux de recherche menés par nos membres. La plupart de ces documents de travail a été soumis à des revues avec comité de révision. Lorsqu'un document est accepté et publié, le pdf original est retiré si c'est nécessaire et un lien vers l'article publié est ajouté.

The series *Les Cahiers du GERAD* consists of working papers carried out by our members. Most of these pre-prints have been submitted to peer-reviewed journals. When accepted and published, if necessary, the original pdf is removed and a link to the published article is added.

CITATION ORIGINALE / ORIGINAL CITATION

F. Malandra, B. Sansò, A simulation framework for network performance evaluation of large-scale RF-mesh AMIs, Simulation Modelling Practice and Theory, 75, 165-181, 2017, https://doi.org/10.1016/j.simpat.2017.04.004.

La publication de ces rapports de recherche est rendue possible grâce au soutien de HEC Montréal, Polytechnique Montréal, Université McGill, Université du Québec à Montréal, ainsi que du Fonds de recherche du Québec – Nature et technologies.

The publication of these research reports is made possible thanks to the support of HEC Montréal, Polytechnique Montréal, McGill University, Université du Québec à Montréal, as well as the Fonds de recherche du Québec – Nature et technologies.

Dépôt légal – Bibliothèque et Archives nationales du Québec, 2017
– Bibliothèque et Archives Canada, 2017

Legal deposit – Bibliothèque et Archives nationales du Québec, 2017
– Library and Archives Canada, 2017

GERAD HEC Montréal
3000, chemin de la Côte-Sainte-Catherine
Montréal (Québec) Canada H3T 2A7

Tél. : 514 340-6053
Téléc. : 514 340-5665
info@gerad.ca
www.gerad.ca

A simulation framework for network performance evaluation of large-scale RF-mesh AMIs

Filippo Malandra
Brunilde Sansò

GERAD & Department of Electrical Engineering, Polytechnique Montréal, Montréal (Québec) Canada, H3C 3A7

filippo.malandra@polymtl.ca
brunilde.sanso@polymtl.ca

March 2016
Revised: April 2017
Les Cahiers du GERAD
G–2016–19
Copyright © 2017 GERAD, Malandra, Sansò

Les textes publiés dans la série des rapports de recherche *Les Cahiers du GERAD* n'engagent que la responsabilité de leurs auteurs. Les auteurs conservent leur droit d'auteur et leurs droits moraux sur leurs publications et les utilisateurs s'engagent à reconnaître et respecter les exigences légales associées à ces droits. Ainsi, les utilisateurs:

- Peuvent télécharger et imprimer une copie de toute publication du portail public aux fins d'étude ou de recherche privée;
- Ne peuvent pas distribuer le matériel ou l'utiliser pour une activité à but lucratif ou pour un gain commercial;
- Peuvent distribuer gratuitement l'URL identifiant la publication.

Si vous pensez que ce document enfreint le droit d'auteur, contactez-nous en fournissant des détails. Nous supprimerons immédiatement l'accès au travail et enquêterons sur votre demande.

The authors are exclusively responsible for the content of their research papers published in the series *Les Cahiers du GERAD*. Copyright and moral rights for the publications are retained by the authors and the users must commit themselves to recognize and abide the legal requirements associated with these rights. Thus, users:

- May download and print one copy of any publication from the public portal for the purpose of private study or research;
- May not further distribute the material or use it for any profit-making activity or commercial gain;
- May freely distribute the URL identifying the publication.

If you believe that this document breaches copyright please contact us providing details, and we will remove access to the work immediately and investigate your claim.

Abstract: Advanced Metering Infrastructures (AMIs) lay the foundation of a wide variety of smart-grid applications. Despite their low capacity, RF-mesh systems are an increasingly popular option for AMI implementation. In this paper, we present a simulation framework for realistic RF-mesh AMIs with the objective of analyzing the performance of this kind of system, and of defining the feasibility of possible smart-grid applications. The framework contains a simulation tool, implemented in Java and Python, that permits the simulation of large-scale AMIs, while taking into account important technical details in a reasonable amount of time. Numerical results obtained in a real case scenario are also proposed and discussed.

Keywords: Wireless Mesh Network, FHSS, ALOHA, performance analysis, RF-mesh

1 Introduction

RF-mesh Advanced Metering Infrastructures (AMIs) are increasingly popular and can be used as a transmission support for different types of smart-grid applications. However, an accurate simulation of RF-mesh AMIs and a proper evaluation of their performance are fundamental to assess the behaviour of the system when all those applications are functional.

Network simulators are usually designed to recreate the performance behaviour of a system taking into account network layer protocols and conditions. Therefore, when working with RF-systems, cross-layer modules have to be integrated into commercial and/or open source simulation tools, in order to be able to study the network layer performance while considering the lower layer functionalities and phenomena. Reviewing the literature on RF-mesh AMI simulators, we found that most works relied on OPNET [1, 2, 3, 4, 5, 6], while others employed NS-2 or NS-3 [7, 8, 9], Contiki OS and its network simulation module Cooja [10, 11, 12], CASTALIA [13], and OMNET++ [14, 15].

OPNET is a commercial network simulator with a user-friendly Graphical User Interface (GUI) and a wide variety of modules to simulate different wired and wireless technologies and protocols. The authors who employed OPNET carefully took into consideration some aspects of AMI implementations, such as routing, propagating condition, QoS requirements; however, the network sizes considered in the published studies were too small to represent the large-scale phenomena of real life RF-mesh AMIs [1, 2, 3, 4, 5, 6].

NS-2 and NS-3 are two very popular open-source discrete-event network simulators that allow for an accurate representation of the physical channel with complex propagation models (i.e., Nakagami-Rayleigh in [8] and HATA COST231 in [9]). Again, only small-size networks (of around 60 nodes) were considered in the two contributions and the time horizon employed was too short (e.g., 20 s in [9]) to provide general considerations on AMI performance. The authors of [7], on the other hand, used 350-node instances but their analysis was focused on the performance of an AMI under a cyber-attack; therefore, they did not deal with general application performance issues.

Contiki is an open-source OS, mainly used to connect small low-cost, low-power micro-controllers to the Internet. It supports a wide range of wireless standards and communication protocols. It also provides Cooja, a network simulator particularly used in the performance analysis of AMI systems. Unfortunately, no module dedicated to RF-mesh technology was found in the literature [10, 11, 12].

CASTALIA, an open-source discrete-event-driven network simulator, was used in [13] to analyze the AMI performance. The instance size was again in the order of few hundred nodes, and the geographical (e.g., location of nodes) and topological (e.g., number of neighbors) aspects of the problem were not considered. Moreover, the performance analysis only encompassed the hop count and an end-to-end delay histogram.

The free discrete-event-driven network simulation software OMNET++ was used in [14], where different routing solutions were compared. Despite the large-scale nature of the instances, in [14] Geographic Information System (GIS) data were not used and the positions of smart meters were randomly distributed in a given area. An inspiring work using OMNET++ is [15], where GIS data were used to build consistent large-scale instances; the authors, however, mainly focused on hop count statistics, providing little detail on some important performance indexes, such as latency or the amount of time spent in transmission by smart meters.

Despite the fact that existing simulation platforms are extensively employed in general networking, some issues and gaps were observed in the RF-AMI performance literature. First, there is a lack of modules dedicated to the RF-mesh technology in affordable off-the-shelf software. Second, some important modelling details such as Frequency Hopping Spread Spectrum (FHSS) (which will be explained in Section 2.2.5) are not implemented. Third, there is an issue of low scalability, as most of the literature papers simulate wireless systems up to few hundreds of smart meters, a consistently lower scale compared to currently implemented RF-mesh AMIs. Moreover, many articles do not focus on the geographical and topological aspects of the problem, which are important to better analyze the peculiarities of RF-mesh AMIs. Finally, there is a lack of publicly available information, which makes it difficult to compare and reproduce different situations and results: some authors do not share details of their simulations, others use software that is not open-source.

As a conclusion, the study of the literature on AMI simulators shows that modifying general purpose networking simulators leads to some important shortcomings that do not allow to capture the performance of large-scale systems. Therefore, we decided to part from the aforementioned studies and avoid implementing yet another module of an existing network simulator. Rather, we propose a new framework that captures the most important performance features while allowing the study of large-scale AMI-systems.

To fill the gap in currently available solutions, we propose a simulation framework with the aim of achieving a detailed performance analysis of large-scale RF-mesh AMI systems. Our methodology permits to calculate the probability of collision of packets and the end-to-end delays in different geographical areas, analyzing possible bottlenecks of the system. Wireless interference and its negative effects on performance are carefully accounted for, as well as other performance indexes, such as the activity time, that can be interesting to limit the public fears on RF exposure. The framework is highly scalable and allows the study of large-scale geographical regions with thousands of smart meters, running different types of applications.

The remainder of this document is structured as follows: the main features of a RF-mesh system are presented in Section 2; the simulation framework is introduced in Section 3, and numerical results obtained with the developed simulation tool are presented in Section 4; Section 5 contains the conclusions and some discussion.

2 Description of the RF-mesh system

2.1 Architecture

Figure 1 shows that RF-mesh AMIs have a layered architecture divided as follows:

- Home Area Network (HAN). This includes electric vehicles, space heaters, water heaters and all the smart appliances within a home and it is characterized by short range communications. All the involved nodes communicate with the smart meter, which acts as a gateway to the upper layers. The main adopted communication technologies are ZigBee and Bluetooth, but also WiFi and Power Line Communications (PLC) are being increasingly used.
- Neighborhood Area Network (NAN). This is a wireless mesh network in which all the smart meters are connected to a data collector. Wireless routers are also installed in order to increase the connectivity and extend the area coverage. The adopted technology is RF-mesh, in which the Industrial Scientific and Medical (ISM) band of 900 MHz is used to transmit data on a mesh topology.
- Wide Area Network (WAN). This is the IP-based backhaul of the communication system: data collectors communicate with the power utility Metering Data Management System (MDMS) by means of satellite and cellular transmissions.

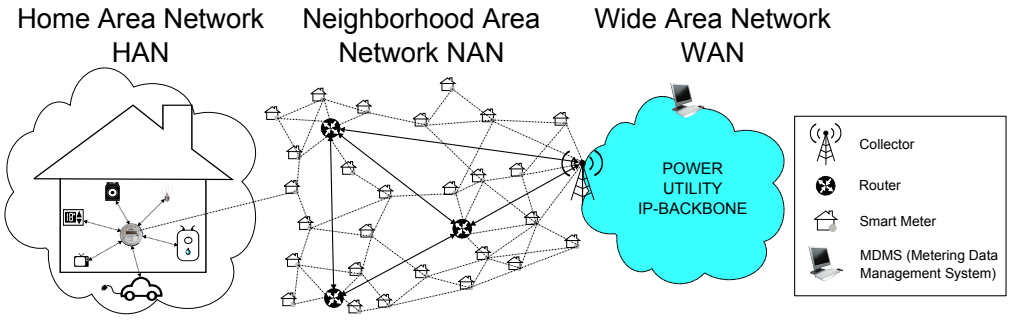

Figure 1: Architecture of the RF-mesh AMI.

The first and the third layers of the architecture (i.e., HAN and WAN) use well-known technologies (e.g., ZigBee or cellular) whose performance has already been extensively investigated in the literature. On the other hand, RF-mesh-system performance has not been as thoroughly studied, and is the topic of this study. The NAN layer of the system under study is composed of:

- *Data collectors*, that are gateways between the NAN and the WAN. They have enhanced radio capacities (e.g., bandwidth, covering ray) with respect to the other nodes. They produce packets directed to the smart meters at a rate that depends on the implemented smart-grid applications.
- *Routers* are devices used as relays between smart meters or between a meter and a data collector. They do not produce their own packets, but are equipped with stronger radio transmitters than those of the smart meters.
- *Smart meters* represent the gateways between the HAN and the WAN; they produce packets towards the data collector at a rate that depends on the implemented smart-grid applications.

2.2 Main features

The main features of the NAN of a RF-mesh AMI to be taken into account in the simulation framework can be summarized as follows.

2.2.1 Large number of nodes

Smart meters are the most numerous devices in the topology: their number ranges from roughly a thousand per neighborhood in a rural environment up to tens of thousands in densely populated urban environments. The number of routers varies according to the considered scenario: in urban instances, very few routers are required since the connectivity of the network is already high, while in rural environments a higher number might be necessary in order to have a fully connected topology, since nodes are otherwise far from each other. The high number of nodes also affects the size of the simulations, increasing the computational burden as the network size increases.

2.2.2 Low throughput

Several factors (e.g., the interference, the use of public frequency bandwidth, and low quality devices) make the nominal rates of the wireless links low, i.e. 19.2 kbps for links between routers and data collectors, and 9.6 kbps for other links (data from [15]). The low throughput hinders the use of RF-mesh AMI for applications that require higher data rates (e.g., video surveillance) but the system under study remains a good candidate for many other applications (e.g., meter reading, load management), which do not need large data transfers.

2.2.3 Black-box nature of the system and undisclosed features

AMI systems are often sold to power utilities as real black-boxes, and very technical details are only provided under strict non-disclosure agreements. Moreover, once installed, smart meter data is considered very sensitive. As a result, some of the characteristics of RF-mesh AMIs are not publicly available, despite their importance for the analysis of the network performance. In the process of designing our framework, we did some reverse engineering and carefully scanned any publicly available piece of information to make the simulator more realistic, while developing the modules as flexible as possible to encompass many different types of undisclosed features.

2.2.4 MAC layer

Two packets that are simultaneously transmitted on the same wireless channel create a *collision*. Wireless systems react in different ways after a collision, depending on the implemented Media Access Control (MAC) layer protocol. In our simulation framework, we considered a smart-meter communication system using a MAC layer based on time-slotted ALOHA. According to this protocol, the time is divided into time slots and a node is allowed to transmit at the beginning of each time slot: therefore, when a node has a packet ready, it waits until the beginning of the following time slot to transmit it. If the correct reception of a given packet i by node A is prevented by a concurrent transmission on the same time slot, node A is *backlogged* and will attempt a retransmission of packet i in one of the following time slots with probability p_r. Despite reducing collision occurrences, the introduction of the retransmission probability degrades the overall performance because it increases the system delay.

2.2.5 Wireless interference issues

As was previously mentioned, AMI RF transmissions take place in a free unlicensed band, where a large number of devices can simultaneously transmit, leading to severe interference issues.

The presence of thousands of potential simultaneous transmitters in a given area requires the adoption of dedicated protocols to mitigate the effect of interference. Among the available protocols, FHSS is one of the most frequently adopted in actual RF-mesh AMIs implementations. The protocol, as shown in Figure 2, consists in subdividing the frequency spectrum into θ sub-frequencies. Signals are then transmitted using just one frequency channel at each time slot. The frequency channel used for transmission varies at each time slot, according to a predetermined sequence that is known and used by all nodes. Two devices interfere with each other if and only if they transmit on the same frequency channel at the same time slot. In order to avoid this, the sequence is shifted over time in each node, in order to reduce the number of neighbors with synchronized sequences. More details on the FHSS implementation can be found in Section 3.3.

FHSS is particularly efficient against the interference coming from other sources (e.g., cordless phones, remote controllers): the power of the interfering signals is spread over the entire available spectrum and their effects on the receiver side are considerably limited. Devices in the same RF-mesh system are considered the only possible sources of interference.

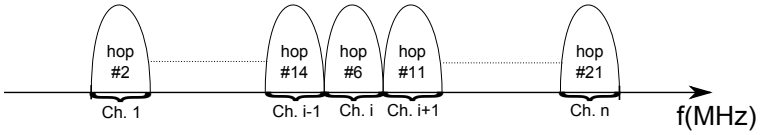

Figure 2: Example of operation of FHSS protocol.

2.2.6 Network layer

An active role in the dynamics of a mesh system is played by the routing protocol, that can greatly impact the network performance. To the best of our knowledge, there is no one prevailing routing mechanism and details about the routing in place in implemented systems are scant. Geographical routing seems to be one of the most popular mechanism in RF-mesh AMIs, but it requires each node to be equipped with a GPS antenna and to know the coordinates of all the other nodes. The so-called *Layer-based* routing is also used in existing systems. In this routing protocol, the word *layer* is used to identify the hierarchical division of the nodes. Every node is assigned a layer number (i.e., collectors are indicated with 0, their neighbors with 1 and so on). The downlink path is decided by the collector based on the information collected in the layer formation phase. On the other hand, each smart meter transmits packets in the uplink direction using one of its neighbors in the upper layer. The advantage of this mechanism is that it is very simple on the smart meter side. Additional details about the routing implementation are provided in Section 3.2.3.

3 Simulation framework

3.1 General structure

In Figure 3, the general structure of the simulator is reported. Three phases are identified: (i) the initialization phase (described in Section 3.2), (ii) the simulation phase (described in Section 3.3), and (iii) the results analysis phase (described in Section 4).

3.2 Initialization phase

The first phase of the simulation framework, schematized in Figure 3, is the *initialization*, whose main objective is to prepare the instance to be simulated. The user is given the possibility to choose the instance that best reflects his/her needs. The flexibility of this phase is key to enable a broad set of performance analyses.

Figure 4 shows that the initialization phase encompasses the nodes placement (described in Section 3.2.1), the link definition (described in Section 3.2.2), and the routing (described in Section 3.2.3).

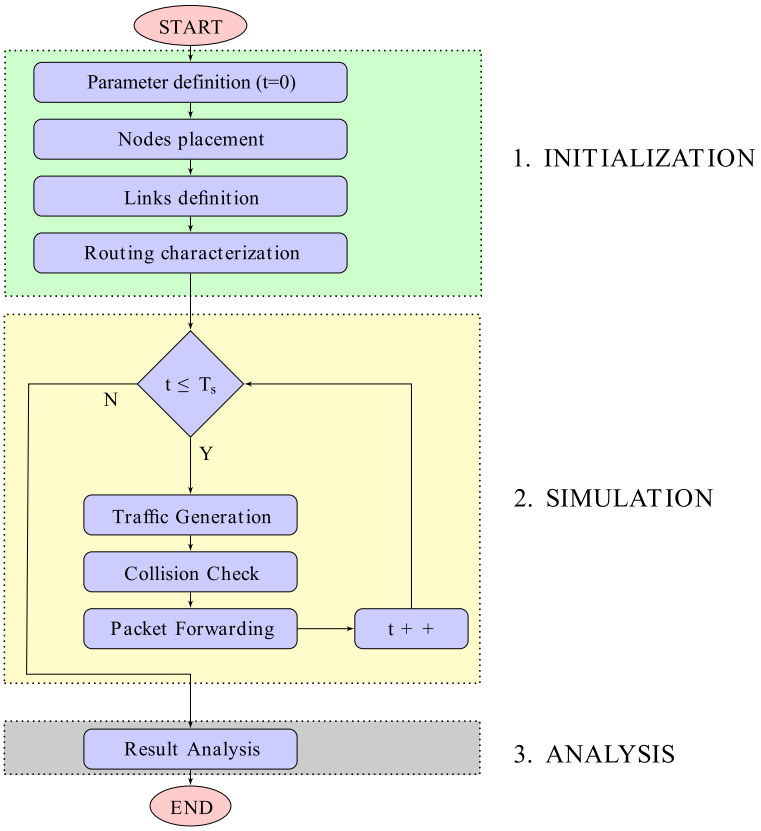

Figure 3: Simplified architecture of the simulator.

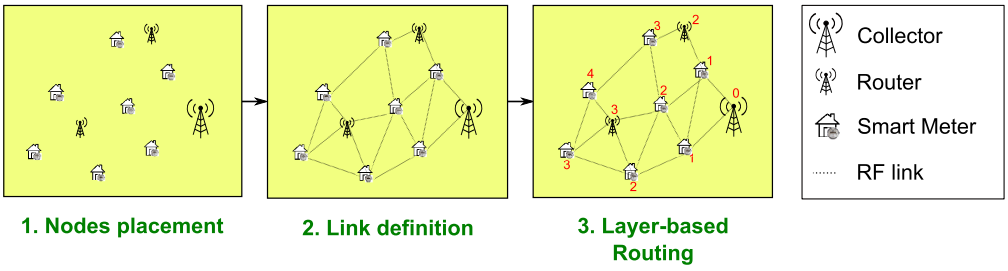

Figure 4: A scheme of the initialization phase with a simple topology with 10 nodes.

Let us define some mathematical notation that will be used in the rest of this section:

V	Set of nodes in the topology
M	Set of smart meter nodes
R	Set of routers
C	Set of data collectors
E	Set of links in the topology
$d(i,j)$	Euclidean distance between node $i \in V$ and node $j \in V$
R_m	Covering ray of each smart meter
R_r	Covering ray of each router and collector
$\nu(i)$	Set of neighbors of node i

3.2.1 Nodes placement

As was already mentioned, three types of devices are used in RF-Mesh AMIs: the smart meters M, the routers R, and the data collectors C. It is important to remark that every device $i \in V$ has a unique functionality and cannot have two different roles nor change its role in the course of a simulation: $M \cup R \cup C = V, M \cap R = M \cap C = C \cap R = \varnothing$. Every node is characterized by: 1) its role, 2) a unique integer ID, and 3) its GPS coordinates. The ID notation follows the convention that the first node is a collector with ID equal to 0. The other IDs are incrementally assigned, starting with any other data collectors, then following with the routers, and finally with the smart meters. At least one data collector is required but, as shown in the rest of the paper, the number of data collectors might be greater than 1.

Nodes position can be either manually selected in a map by means of a geographical tool we implemented, or directly provided in a text file. The manual selection process does not apply to smart meters, for their number is too large (i.e., on the order of thousands); it is rather more convenient to retrieve their position by one of the various portals providing open GIS data (data for the Montreal island, used in our numerical results, can be retrieved from [21]). On the other hand, the position of routers and collectors can be not only selected on a map, but also optimally determined by integrating a facility location model into the current framework, which we are currently studying.

In Figure 5, an example of the topology creation procedure is illustrated. The user can draw a polygon to define the analyzed area (see Figure 5a), then we implemented a script that allows to identify the smart meters located within the selected area; finally, the user is required to select on the map the position of routers (see Figure 5b) and data collectors (see Figure 5c).

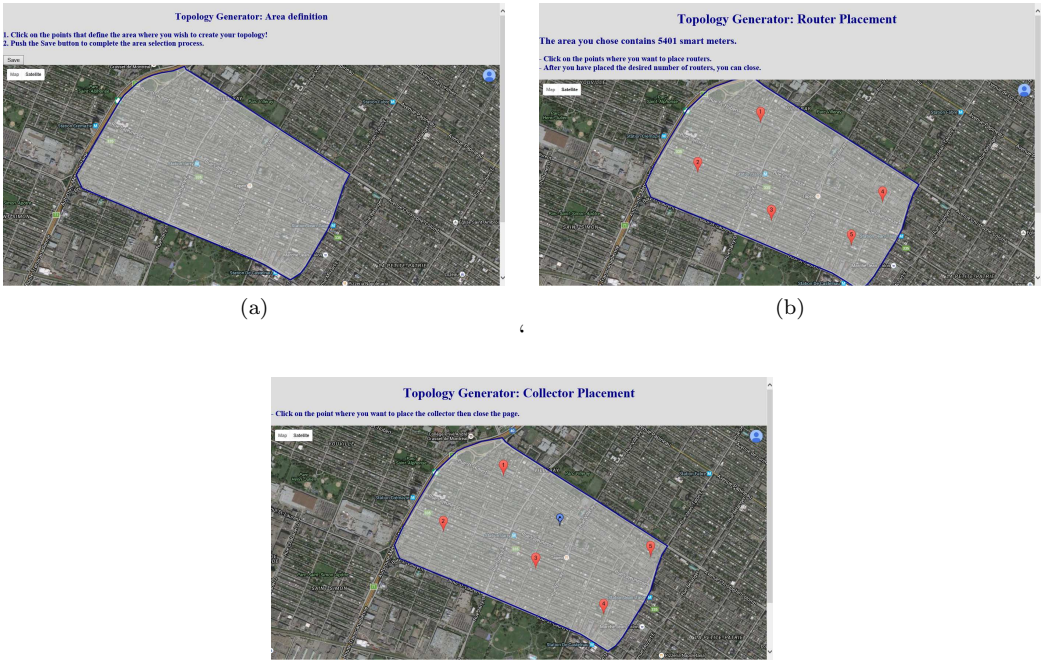

(a) (b)

(c)

Figure 5: Illustration of the topology creation with the definition of a new area (Figure 5a), the choice of routers (Figure 5b), and collectors (Figure 5c).

3.2.2 Link definition

The topology is completed with the definition of the set E of links. In order to keep the complexity low, the definition of the links is based on the euclidean distance between nodes. Two different covering rays were defined: R_m for the smart meters, and R_r for the routers and collectors. Numerical values of R_m and R_r vary

according to the scenario considered: the covering rays are typically shorter in urban scenario than in rural environments, due to the harsh propagating condition (i.e., many many obstacles exist in the path) and the concurrent transmissions of other wireless users in the same unreserved bandwidth. Moreover, the covering ray of the routers and collectors is considerably higher than the covering ray of smart meters because of the use of better antennas and also because routers and collectors can exploit better propagating conditions (they are usually installed on the top of buildings).

E is the set of links (i, j) characterized as follows:

$$E = \{(i,j) : (i,j \in V) \wedge (d(i,j) \leq R_m \wedge i,j \in M) \vee (d(i,j) \leq R_r, (i \in R \cup C) \vee (j \in R \cup C))\} \quad (1)$$

where $d(i, j)$ is the euclidean distance between node i and j, calculated using the GPS coordinates of the nodes according to the Cosine-Haversine formula [16]. In other words, there is a link between i and j if they both are smart meters and their distance is lower than R_m, or if at least one of them is a router or a collector and their mutual distance is lower than R_r.

3.2.3 Routing

In RF-mesh systems, packets flow in just two directions: uplink (from a smart meter to a data collector) and downlink (from a collector to a smart meter). The communication between two smart meters is not possible for confidentiality reasons: messages are encrypted with a key that is shared between the data collector and each smart meter. The routing mechanism is the so-called *layer-based routing*, similar to the one presented in [17]. An initial *layer-formation* process is required to assign a *layer index* to each node. The *layer-based* routing relies on the *layer-updates*, small packets that are used in order to maintain the routes (from smart meters to data collectors and vice versa) up-to-date and to react to possible changes in the topology (e.g., link losses, node failures). For instance, in case a given node i with layer k attempts a transmission to a $(k-1)$-layer node, which becomes unavailable, i will choose one of its neighbors with the lowest layer number, and a path to the collector can be promptly re-established. In case no $(k-1)$-layer neighbor is active, node i chooses one of the neighbors with a higher layer index.

For the sake of illustration, in Figure 4, a scheme of the *initialization* phase is reported for a simple topology with 10 nodes. As shown in the third subfigure, a layer index is assigned to each node. The path in the downlink direction is determined by the collector, based on the updated information received in the *layer updates*. In the uplink direction, the path is not known in advance by the source of the communication: a given smart meter with layer index k transmits the uplink packet to one of its $(k-1)-$layer neighbors. This routing mechanism is a good candidate for AMI systems because it does not require a high computational burden at the smart meter side. Nevertheless, it is dynamic, robust and capable of reacting to topology changes.

3.3 Simulation phase

A scheme of the logical structure of the nodes is reported in Figure 6: each node is equipped with 1) two logical antennas, 2) a FHSS module, 3) two separate buffers (one for incoming packets and one for packets waiting to be transmitted), 4) a packet analyzer, 5) a routing mechanism. However, the elements in the grey area (i.e., destination and traffic generator) are not implemented in routers, but only in smart meters and collectors, which can be sinks or sources of traffic. The two antennas (one for receiving and one for transmitting) are modeled as two logical entities associated to the same physical antenna each node is equipped with. The presence of two logical antennas in the simulator is needed to allow for the possibility to work with one frequency in reception and another in transmission.

Let $F_r(j, t)$ and $F_t(j, t)$ be the frequency channels of the two antennas (respectively, receiver and transmitter) of node j at time t. $F_r(j, t)$ is determined according to the FHSS sequence, known to all the nodes. A given node i, at the beginning of a time slot, can be either in *idle* state or in *transmission* state. When in idle state, it is waiting to receive a packet and its antenna is tuned to the frequency $F_r(i, t)$. On the other hand, when in transmitting state, the transmitting frequency of node i at time t ($F_t(i, t)$) depends on the destination of the transmission: if node i wants to transmit a packet to node j at time t, it must tune

its transmitting frequency to the receiving frequency of node j at time t, namely $F_t(i,t) = F_r(j,t)$. This mechanism is implemented to reduce the chances of collision: a collision in the transmission from node i to node j happens when another neighbor of node j is transmitting on the same channel $F_r(j,t)$.

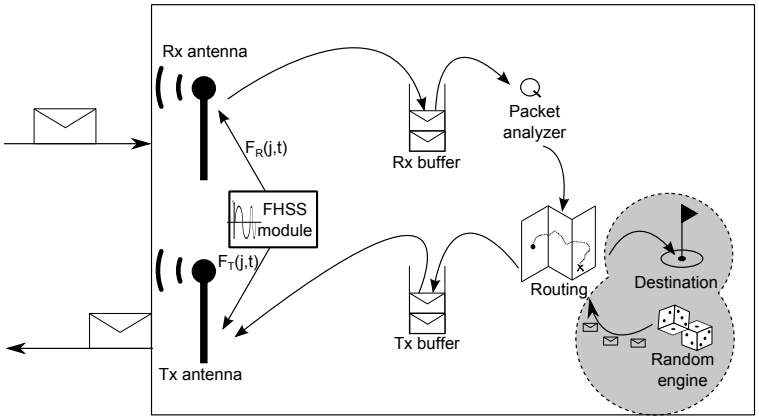

Figure 6: Logical structure of the different types of nodes in the simulator.

The simulation phase, as shown in Fig. 3, consists in the iteration, over the simulation horizon T_s, of three sub-phases (i.e., traffic generation, collision check, and packet forwarding) that are described in detail in the next sections. The simulation phase is *time-driven*, meaning that T_s is subdivided into time slots of duration τ, and a variable is used to record the current time, which is incremented as all the aforementioned phases are performed. An event-driven approach is usually preferred when the number of events is considerably lower than the number of time steps in the simulation. However, the large number of nodes and possible events in the system under study (e.g., reception/transmission of a packet, collisions, buffer updates) made us prefer a time-based approach.

3.3.1 The traffic generator module

At the beginning of each time slot, all the nodes that are equipped with a *traffic generator* can produce a packet according to a random distribution that depends on the type of the implemented applications.

Let us denote by $\Omega = \{\alpha, \beta, \gamma\}$ the set of three different traffic types in the communication system under study. In this case, we have considered meter-reading, demand, and broadcast traffic.

- α (*meter-reading*) consists in the transmission of a packet from a smart meter to its associated collector. This event is Poisson-distributed with parameter λ_u.
- β (*demand*) consists in the random transmission of packets from a data collector to one of its controlled meters. The generation of a packet is also Poisson-distributed (mean parameter λ_d).
- γ (*broadcast*) consists, in general, in the transmission of the same packet from a data collector to all smart meters. In practice, broadcast transmissions, not possible because of privacy requirements, are replaced by unicast packets; nonetheless, in the rest of this paper we will refer to γ as a *broadcast* transmission.

Note that α flows in the uplink direction, while β and γ take place on the downlink. In Figure 7 we reported a screenshot of the mask to set up the initial parameters of the simulation. The three traffic sources (i.e., α, β, and γ) can be selected by means of the corresponding check-boxes, which were circled in the illustration.

The analysis of different kind of applications in the same communication infrastructure can be handful from the point of view of a power utility. Smart grid is constantly enlarging its application domain and the possibility of using only one communication system for a broad set of applications is particularly sought by power utilities.

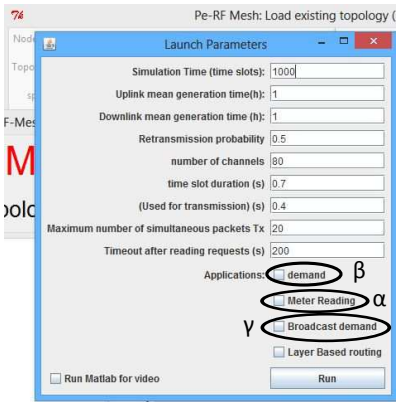

Figure 7: Mask used to set up initial parameters to launch a simulation. The different traffic generation parameters are circled and labeled with the corresponding letter, defined in Section 3.3.1.

3.3.2 The collision check module

When a given node i is attempting a transmission to one of its neighbors $j \in \nu(i)$, possible interferers of the transmission $i \to j$ are all the nodes $k \in \nu(j) : k \neq i, j$ who transmit on the same frequency channel as i. In order to identify the collisions, the dedicated *collision-check* module was implemented. At each time slot, a special check is made to see if any of the transmitting nodes is interfering with each other. Each transmission is identified by a boolean *collision-flag* variable, whose default value is *false*. When a packet collides, its *collision-flag* variable is set to *true* and the packet is scheduled for retransmission at one of the following time slots.

3.3.3 The Packet-forwarding module

At the end of each time slot, after the *traffic generator* module has decided which nodes are transmitting and after the *collision-check* module has determined the presence of collisions, it is necessary to update the Tx and Rx buffers. For this, we implemented the *Packet-forwarding* module. For each transmission from node i to node j, this module checks if a collision has been reported. Then, in case of collision, the packet stays in the Tx buffer of node i and a new transmission will be retried in one of the following time slots with probability p_r. In case no collision was observed, the packet is deleted from the Tx buffer of node i and forwarded to the Rx buffer of node j. Then the *packet-analyzer* (see Figure 6) of node j verifies the destination of the packet: if node j is the destination, the packet is considered successfully received and packet statistics are updated; if node j is not the destination, the packet will be passed to the *routing* module, in order to determine the next hop, and written to the Tx buffer of node j.

3.4 Randomness in the simulator

Random number generation is a key element in computer-aided simulations and is usually performed by means of the so-called *random engines*, objects that can generate numbers according to different types of distributions (e.g., uniform, beta, exponential). Those engines, regardless of the operating system and of the used programming language, adopts computational algorithms to generate pseudo-random sequences, which are based on an input parameter, called *seed*. The use of random engines and initial seeds guarantees the possibility of re-running simulations, and enables analyses on the truthfulness of the simulation results. Figure 8 illustrates how the random engines of the nodes are initialized. As shown, a central random engine is used to generate the seeds for all the random engines in the simulator. Each random engine generates traffic according to the mean packet generation rate of smart meters and data collectors (i.e., respectively λ_u and λ_d).

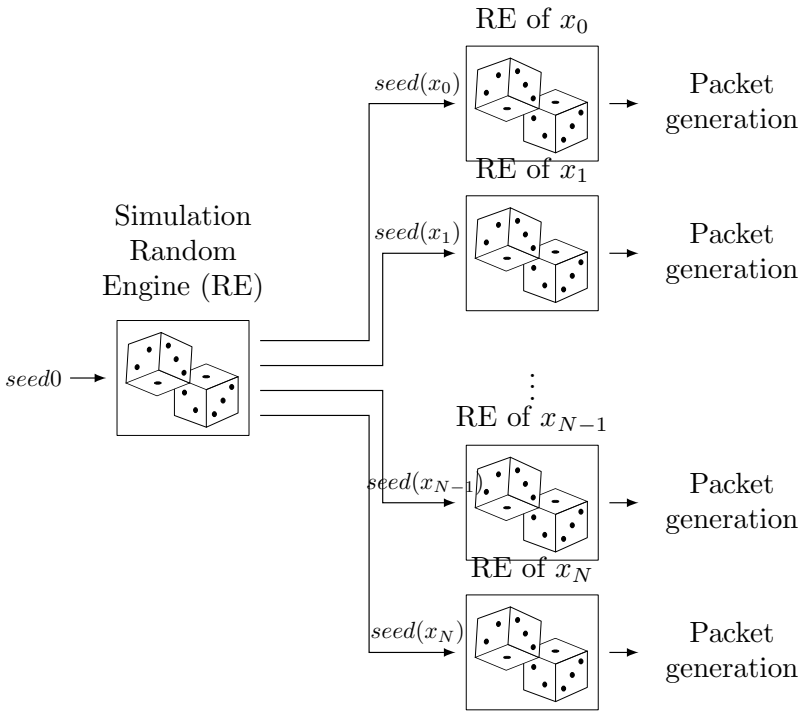

Figure 8: Illustration of the seed initialization and of the random packet generation in the simulator.

4 Numerical results

To illustrate the interest and versatility of the proposed framework, we present in this section a set of results that were obtained by analyzing collision probability, delay and smart-meters activity time in a realistic setting built from publicly available data.

The scenario used to produce this set of numerical results is based on Villeray, a neighborhood within the city of Montreal, which was one of the three areas chosen for a pilot project of smart meter installation in Québec [18]. The starting topology was created with the topology generator described in Section 3.2. In particular, the position of routers and collectors were extracted from [18] and stored into a text file. The GPS coordinates of smart meters, not provided in the previous document, were extracted in an automated way by a dataset[1] containing all the residential addresses in the city of Montreal and stored in a text file as well. The text files with the GPS coordinates of the nodes are used as input of the topology generator. The topology is composed of 2 data collectors, 16 routers, and 6033 smart meters over an area of 2.7 km^2. In our simulations, we created 20 traffic scenarios with $1/\lambda_u = 1, 0.5, 0.25, 0.125$ h and $1/\lambda_d = 4, 3, 2, 1, 0.5$ h and no broadcast transmission. The effect of broadcast traffic on the performance was studied in 20 additional traffic scenarios with the same values of $1/\lambda_u$ and $1/\lambda_d$, but adding one broadcast transmission per day at a predetermined time slot. Relevant parameters that affect the simulation results are τ (i.e., the time slot duration), C_r and C_m (i.e., respectively the capacity of links between routers/collectors, and the capacity of all other links), L (i.e., the packet size in Bytes), and Θ (i.e., the buffer size expressed in number of packets). The average number of packets that can be simultaneously transmitted on the links between routers/collectors can be found as $\phi_r = C_r\tau/L$, and on the other links it is $\phi_m = C_m\tau/L$. In the case under study, given that $C_m = 9.6$ kbps, $C_r = 19.2$ kbps, $\tau = 0.7$ s and $L = 100$ Bytes $= 800$ bits, we have $\phi_r = 16.8$ packets and $\phi_m = 8.4$ packets.

[1] Provided by *Portail Données Ouvertes Montreal*, available at http://donnees.ville.montreal.qc.ca/dataset/adresses-ponctuelles

Additional notation, used in the rest of this section, is reported below:

$N_t(i)$	total number of transmissions of node $i \in V$
N_t	overall number of transmissions
$N_c(i)$	total number of collisions experienced by node $i \in V$
N_c	total number of collisions
$\pi(i)$	collision probability at node i
π	overall collision probability

4.1 Confidence interval analysis and results reliability

For every traffic scenario, we performed 50 simulations (i.e., we used 50 different initial seeds $seed_0$) in a 7-day time horizon. The use of multiple initial seeds permits to calculate confidence intervals for the parameters that are presented in this section. If we denote by $k = 1..50$ the set of initial seeds, and by $X^{(k)}$ the observation of a random variable X when the initial seed is equal to k, we can compute:

$$m = E[X^{(k)}] = 1/50 \sum_{k=1}^{50} X^{(k)}, \qquad s^2 = var(X^{(k)}) = 1/50 \sum_{k=1}^{50} (X^{(k)} - m)^2 \tag{2}$$

and use them to compute the confidence interval at the 95% confidence level as $E[X^{(k)}] \pm 1.97s$. In this case, 95% represents the reliability of the estimation of the real mean μ of the random variable X, which is unknown.

4.2 Collision probability

One of the elements that most affect the performance of a wireless network is the mutual interference of transmitting nodes. FHSS protocol mitigates the effects of wireless interference by increasing the number of communication channels and consequently reducing the chances of collisions, as shown in [19, 20]. However, collisions are not completely eliminated because of the limited number of available channels and the high number of neighbors, and consequently interferers, each node has in RF-mesh AMIs.

Numerical results on the collision probability π are summarized in Table 1 for the 20 simulations run with simulation time $T_s = 864010$ time slots (roughly 7 days). In the Table, the 95% confidence intervals for values for π are reported according to the different values of λ_u and λ_d used in the simulations. Note that the average collisions probability ranges from 1.77% (in the scenario with $1/\lambda_u = 1$ hour and $1/\lambda_d = 4$ hours) to 9.21%(in the scenario with $1/\lambda_u = 0.125$ hour and $1/\lambda_d = 0.5$ hours) in the scenarios without broadcast transmissions. Moreover, the introduction of one broadcast transmission per day does not seem to increase the overall the collision probabilities which range from 1.92 % to 9.28 %.

One of the simulated scenarios (i.e., with one broadcast transmission per day, $1/\lambda_d = 0.5$ h, and $1/\lambda_u = 0.125$ h) has been studied separately in the rest of this section. A more accurate portrait of the dynamics of the network in the aforementioned scenario is shown in the heat-map of the collision probabilities in Figure 9. The two heat-maps do not considerably differ: the slightly higher collision probability in downlink can be remarked by looking at the difference between the two color-bars. The perimeter of the analyzed area was also drawn in order to highlight the area analyzed in the simulation. Even though the average collision percentage of all nodes is always low, according to Table 1, from Figure 9 we can see that the situation is considerably different in the surroundings of the 2 data collectors: a high number of collisions is experienced and very high collision probabilities are observed. The reason behind the increased number of collisions is to be found in the higher concentration of packet transmissions, in both uplink and downlink directions, in that area.

Table 1: 95% confidence intervals of the average collision probability (π) according to different levels of $1/\lambda_u$ (rows) and $1/\lambda_d$ (columns).

	Collision probability π (%)			
$1/\lambda_d$ (hours)	$1/\lambda_u$ (hours) 1	0.5	0.25	0.125
4.0	**1.77±0.24**	3.08±0.41	5.13±0.84	7.50±0.98
3.0	1.93±0.29	3.26±0.40	5.31±0.79	7.75±1.12
2.0	2.22±0.38	3.51±0.49	5.66±0.79	7.93±1.20
1.0	2.83±0.37	4.22±0.60	6.38±0.97	8.84±1.37
0.5	3.30±0.45	4.67±0.73	6.78±0.98	**9.21±1.39**
	Collision probability π (%) - with broadcast traffic			
$1/\lambda_d$ (hours)	$1/\lambda_u$ (hours) 1	0.5	0.25	0.125
4.0	**1.92±0.31**	3.12±0.47	5.16±0.73	7.48±0.92
3.0	2.06±0.30	3.26±0.41	5.40±0.73	7.76±1.14
2.0	2.30±0.35	3.54±0.53	5.57±0.83	7.91±1.02
1.0	2.89±0.42	4.29±0.62	6.44±0.90	8.86±1.40
0.5	3.29±0.49	4.66±0.79	6.95±1.01	**9.28±1.54**

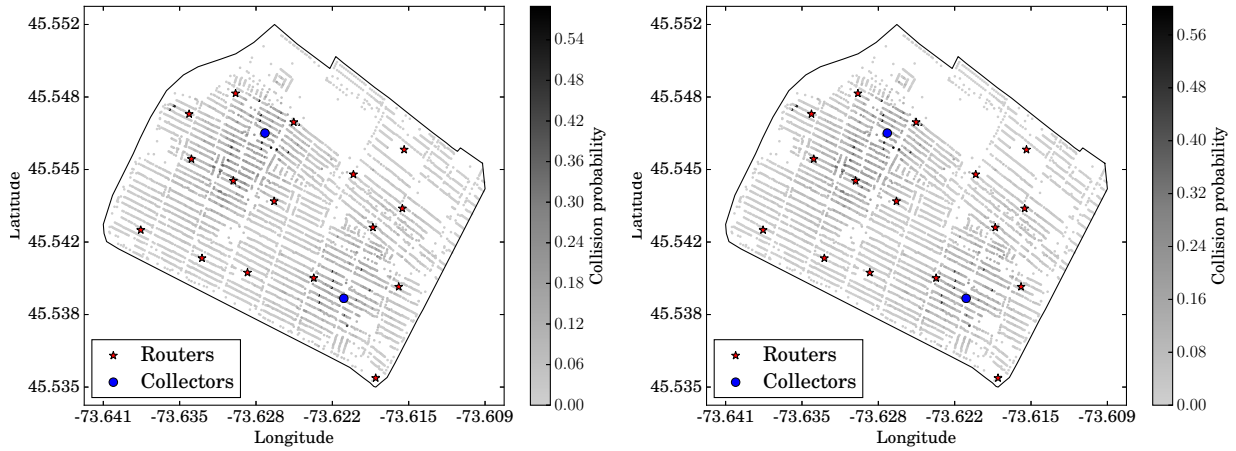

(a) without broadcast (b) with broadcast

Figure 9: Heat-map of the collision probability in the scenario with $1/\lambda_d = 0.5$ h, and $1/\lambda_u = 0.125$ h.

4.3 Delay analysis

Delay is one of the most important indexes of network performance. If we denote with $T_d(k)$ the generation time slot of packet k and with $T_a(k)$ the arrival time slot at its destination, we can generally define the delay $D(k)$, encountered by packet k, throughout the network as:

$$D(k) = T_a(k) - T_d(k) + 1 \tag{3}$$

It is also important to separately study the average delay for the uplink and downlink traffic streams, respectively $D_\alpha(i)$ and $D_\beta(i)$.

As was done for the collision probability, we carried out a 95% confidence interval analysis of the delay not considering broadcast traffic. In the upper part of Table 2, we reported the values of D_α and D_β without broadcast transmissions, according to the previously defined ranges of variation of $1/\lambda_d$ and $1/\lambda_u$. As one can see, the delay in uplink (D_α) slightly decreases as the packet generation rate increases, but in the downlink direction (i.e., D_β) higher delays are experienced, as also illustrated in Figure 10. In particular, we can notice that when the mean packet generation time in downlink goes below 1 h, there is a steep increase in the average downlink delay, with values ranging from 34.89 s to 45.16 s.

Table 2: 95% confidence intervals of the average delay (expressed in seconds) for the different types of traffic.

	D_α (s)				D_β (s)			
$1/\lambda_d$ (hours)	$1/\lambda_u$ (hours) 1	0.5	0.25	0.125	1	0.5	0.25	0.125
4.0	**6.48**±0.03	6.57±0.03	6.71±0.07	6.90±0.09	**6.79**±0.16	6.92±0.13	7.18±0.14	7.47±0.17
3.0	6.49±0.03	6.58±0.03	6.73±0.06	6.92±0.10	6.91±0.15	7.08±0.16	7.41±0.27	7.69±0.22
2.0	6.52±0.03	6.61±0.03	6.76±0.07	6.94±0.13	7.33±0.24	7.53±0.27	7.90±0.34	8.29±0.41
1.0	6.59±0.03	6.68±0.05	6.84±0.08	7.05±0.13	10.75±0.77	11.73±1.42	13.19±1.54	15.52±2.17
0.5	6.64±0.04	6.73±0.06	6.89±0.08	**7.10**±0.13	34.89±1.48	37.24±1.89	41.18±2.34	**45.16**±3.21
	D_α (s) - with broadcast traffic				D_β (s) - with broadcast traffic			
$1/\lambda_d$ (hours)	$1/\lambda_u$ (hours) 1	0.5	0.25	0.125	1	0.5	0.25	0.125
4.0	**6.48**±0.02	6.57±0.04	6.71±0.06	6.90±0.08	**7.62**±0.17	7.81±0.16	8.15±0.20	8.51±0.24
3.0	6.50±0.02	6.58±0.04	6.74±0.06	6.93±0.10	7.78±0.19	8.00±0.22	8.35±0.16	8.74±0.22
2.0	6.52±0.03	6.61±0.05	6.76±0.06	6.94±0.10	8.19±0.28	8.43±0.24	8.85±0.29	9.45±0.46
1.0	6.59±0.03	6.68±0.04	6.84±0.07	7.05±0.13	11.64±0.85	12.67±1.31	14.27±1.23	16.50±1.87
0.5	6.64±0.04	6.73±0.06	6.91±0.07	**7.11**±0.15	35.49±1.57	37.97±1.90	42.54±2.33	**46.90**±3.68

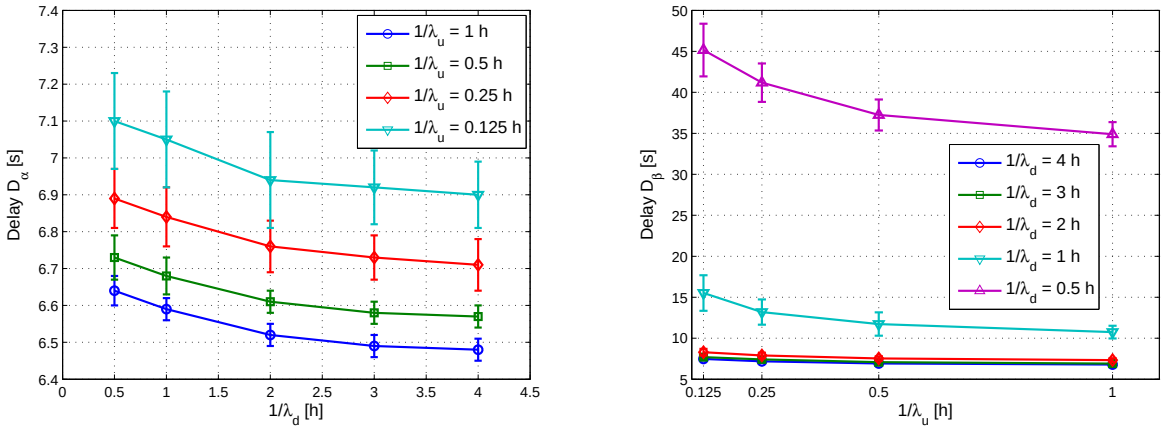

(a) D_α (b) D_β

Figure 10: Confidence intervals for D_α and D_β traffic without broadcast traffic.

In Figure 11, we reported the two heat maps of the delays (uplink in Figure 11a and downlink in Figure 11b) in the scenario with one daily broadcast transmission, $1/\lambda_d = 0.5$ h and $1/\lambda_u = 0.25$ h.

Note that the average delay in the downlink direction is considerably higher than in the uplink (i.e., $D_\beta = 6.89$ s, $D_\alpha = 41.18$ s): this confirms that the packet generation rate in the downlink has a higher impact on the delay, with respect to its uplink counterpart. Another remarkable element is that downlink delay tends to be more homogeneous than uplink delay. Besides the visual representation of this behavior from the maps of Figure 11, we defined and calculated the delay variation coefficients σ_u^* and σ_d^*, for respectively the uplink and the downlink. These are defined as the ratio between the standard deviation and the average, and their computation for this scenario gives $\sigma_u^* = 0.495$ and $\sigma_d^* = 0.140$. The reason behind the higher homogeneity of the downlink direction can be found in the increased link congestion in the surroundings of the data collectors. Nodes in these areas suffer from the proximity to the collector and its limited buffer size, that causes additional waiting times to the packet transmission.

Continuing the analysis, we investigated the impact of broadcast transmissions (see lower part of Table 2) on the delay of the α and β traffic. We can notice that the uplink communications are not sensitively affected by the introduction of a broadcast transmission: the interval of D_α spans from 6.48 s to 7.11 s (whereas, the variation range without broadcast was from 6.48 s to 7.10 s. On the other hand, a small increase in D_β

is observed: suffice it to compare its average values in the case with broadcast (i.e., from 7.62 s to 46.90 s) to the corresponding average values without the broadcast (i.e., from 6.79 s to 45.16 s). D_γ resulted to be considerably higher than D_α and D_β, with average values upper than 5 minutes.

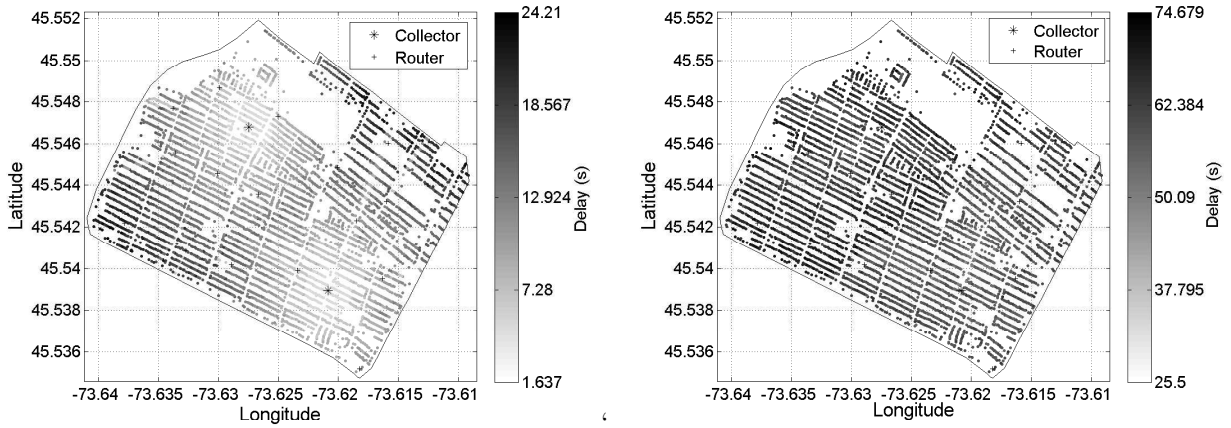

(a) D_α (b) D_β

Figure 11: Heat-map of the delay in the scenario with one broadcast transmission per day, $1/\lambda_d = 0.5$ h and $1/\lambda_u = 0.25$ h.

4.4 Activity time percentage

Another sensitive index in the context of smart meter performance analysis is the activity time percentage $\chi(i)$, which represents the fraction of the simulated time in which node i is actually transmitting a packet. The importance of this parameter is driven by the recent concerns about the electromagnetic impact on public health, issued by the massive installation of smart meters in residential premises. The average activity time χ of all nodes can be computed as follows:

$$\chi = \frac{\sum\limits_{\forall i \in V} \chi(i)}{|V|} = \frac{\sum\limits_{\forall i \in V} N_t(i)}{T_s\,|V|} \tag{4}$$

Since χ takes into account all the nodes in the network, and since the main concerns are related to the smart meters, we decided to define 3 additional indexes, χ_m, χ_r, and χ_c, representing the average activity time percentage of respectively smart meters, routers, and data collectors, which are computed as follows:

$$\chi_m = \frac{\sum\limits_{\forall i \in M} \chi(i)}{|M|} = \frac{\sum\limits_{\forall i \in M} N_t(i)}{T_s\,|M|} \tag{5}$$

$$\chi_r = \frac{\sum\limits_{\forall i \in R} \chi(i)}{|R|} = \frac{\sum\limits_{\forall i \in R} N_t(i)}{T_s\,|R|} \tag{6}$$

$$\chi_c = \frac{\sum\limits_{\forall i \in C} \chi(i)}{|C|} = \frac{\sum\limits_{\forall i \in C} N_t(i)}{T_s\,|C|} \tag{7}$$

95% confidence intervals for χ_m, χ_r and χ_c are reported in Table 3. We can notice that, as expected, the activity time percentage increases as the packet generation rates increase: we observe that the variation of the activity time percentage with respect to the variation of $1/\lambda_d$ is much more evident than with respect to the variation of $1/\lambda_u$. However, numerical values of χ_m are always between 0.103 and 0.522 %: this is interesting because it can be used to reply to the public concerns about an excessive human exposure

to wireless waves produced by smart meters. In fact, our results show that this kind of devices were in transmission mode for only a very low percentage of time, much lower than many others wireless devices used in everyday life, such as smartphones, and cordless phones. Particularly interesting is also the mean activity time of data collectors: in all the scenarios with $1/\lambda_d = 0.5$ h, the data collectors are active for 50% of the time, on average.

Table 3: Average activity time percentages for smart meters (χ_m), routers (χ_r) and data collectors (χ_c) for the different type of traffic according to different levels of $1/\lambda_u$ (rows) and $1/\lambda_d$ (columns) without broadcast style traffic.

	χ_m (%)			
$1/\lambda_d$	$1/\lambda_u$ (hours)			
(hours)	1	0.5	0.25	0.125
4.0	**1.03e-1±3.63e-4**	1.87e-1±1.04e-3	3.29e-1±3.66e-3	4.59e-1±7.94e-3
3.0	1.08e-1±3.89e-4	1.93e-1±1.04e-3	3.34e-1±3.48e-3	4.65e-1±8.88e-3
2.0	1.18e-1±4.61e-4	2.02e-1±1.15e-3	3.44e-1±4.11e-3	4.75e-1±1.13e-2
1.0	1.39e-1±4.98e-4	2.25e-1±1.58e-3	3.69e-1±4.36e-3	5.02e-1±1.13e-2
0.5	1.60e-1±7.95e-4	2.45e-1±1.68e-3	3.89e-1±4.20e-3	**5.22e-1±8.48e-3**
	χ_r (%)			
$1/\lambda_d$	$1/\lambda_u$ (hours)			
(hours)	1	0.5	0.25	0.125
4.0	1.08±7.19e-3	1.30±1.20e-2	1.68±4.03e-2	2.04±7.86e-2
3.0	1.34±8.63e-3	1.58±1.63e-2	1.97±3.94e-2	2.35±1.07e-1
2.0	1.84±1.75e-2	2.08±2.21e-2	2.50±4.81e-2	2.89±9.85e-2
1.0	3.03±3.26e-2	3.29±5.41e-2	3.73±6.53e-2	4.17±1.36e-1
0.5	3.57±7.45e-3	3.78±1.89e-2	4.14±3.46e-2	**4.50±7.46e-2**
	Activity time of data collectors: χ_c(%)			
$1/\lambda_d$	$1/\lambda_u$ (hours)			
(hours)	1	0.5	0.25	0.125
4.0	14.8±8.94e-2	15.1±1.60e-1	15.6±2.37e-1	16.1±3.38e-1
3.0	19.3±1.65e-1	19.7±1.97e-1	20.3±4.07e-1	21.0±4.80e-1
2.0	27.5±3.06e-1	28.1±2.88e-1	29.0±4.83e-1	30.0±7.53e-1
1.0	45.7±5.27e-1	46.2±9.75e-1	47.2±7.94e-1	47.9±7.68e-1
0.5	**50±5.97e-2**	**50±5.88e-2**	**50±1.75e-1**	**50±3.78e-2**

4.5 Computational time

RF-mesh systems are usually large-scale with thousands of nodes, therefore the computational burden can be a serious impairment to simulation and needs to be carefully taken into account. With the presented simulation framework, the average time to perform a simulation of 6051-node instances over a simulated time of 7 days was of around 30 minutes, on a machine with a *AMD A8-4500M CPU* working at 1.90 GHz. This is a very important result because it proves the capacity to simulate large-scale systems in a considerably short time.

4.6 Scalability analysis

When it comes to simulating extended systems, such as the RF-Mesh AMIs, it is fundamental to use tools that can easily scale up the number of nodes: computational efficiency is therefore fundamental. In order to analyze it, we created a set of 16 topologies, ranging from 1715 to 20798 nodes, as shown in Table 4. A visual representation of the 16 topologies, created by means of the topology generation tool described in Section 3.2.1, is reported in Figure 12. As can be seen, the topologies were created in the same geographical area (i.e., the Villeray neighborhood in Montreal) so that their neighborhood characteristics are preserved, in particular node density.

Table 4: Details about the topologies used in the scalability analysis.

ID	nr. of nodes	Smart meters	Routers	Collectors
1	1715	1712	2	1
2	2388	2385	2	1
3	3126	3122	3	1
4	4187	4183	4	1
5	4786	4782	5	1
6	5372	5367	5	1
7	6581	6574	6	1
8	7872	7865	7	2
9	9119	9108	9	2
10	10393	10381	10	2
11	11917	11904	11	2
12	13660	13645	13	2
13	15755	15738	15	2
14	17923	17905	17	3
15	19994	19974	19	3
16	20798	20775	20	3

Figure 12: A visual representation of the 16 topologies created for the scalability analysis. Details about the topology can be found in Table 4.

The topologies were used to perform $7 - day$ simulations, whose computational times are reported in Figure 13. The same simulation settings were used in the 16 simulations in order to have similar traffic patterns (i.e., $1/\lambda_d = 0.5$ h, $1/\lambda_u = 0.25$ h, and $p_r = 0.5$) so that the variation of the computational time with respect to the number of nodes can be evaluated. A quasi-linear growth of the computational tie is observed. We computed the quadratic regression of the computational times with respect to the number of nodes and the result was the following 2^{nd} degree polynomial:

$$y = 7.009 \cdot 10^{-6} x^2 + 0.285x - 136.31 \tag{8}$$

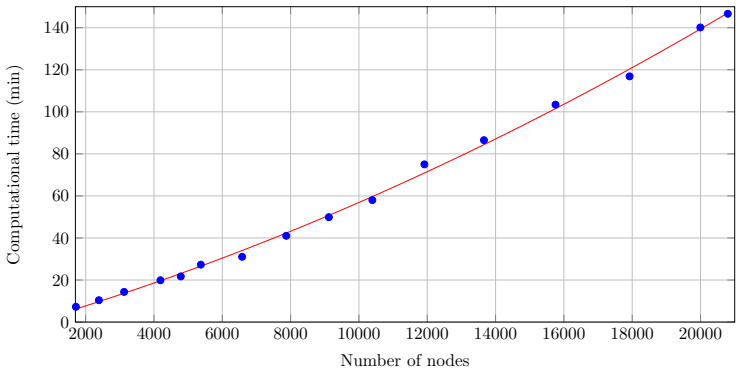

Figure 13: Computational time to perform a 7-day simulation using topologies with a number of nodes ranging between 1718 and 20798. The quadratic regression is reported in red.

The very low 2^{nd} degree coefficient explains the low concavity of the quadratic regression curve and the quasi-linear behavior of the computational time with respect to the number of nodes, in the analyzed domain (between 1715 and 20798).

5 Conclusion

As smart grids proliferate around the world and AMI systems are widely deployed, more and more applications will likely be introduced. Therefore, it is essential for the power utilities to have appropriate tools to be able to assess the performance of the system and the impact of new applications on it. In this paper, we have presented a framework to assess the performance of AMI systems that removes some of the limitations of previous work related to AMI performance, such as scalability or adaptability.

The framework yielded an effective simulation tool that allows for great flexibility in the selection of system features (e.g., the area under consideration, the number of nodes). The implemented topology generation tool grants the possibility to create customized instances, and allows both to manually choose the location of routers and collectors, and to be combined to an optimization tool for the location of routers and data collectors. The observed computational efficiency permits the analysis of instances of thousands of nodes in a very reasonable time.

The numerical results used to illustrate the framework capabilities have nonetheless brought to light some useful insights into the AMI system in a densely populated NAN. There is a performance degradation in the surroundings of the collectors, where multiple traffic streams coexist and mutually disturb each other. Difficulties in the handling of broadcast traffic were observed, but the uplink delay is not particularly affected by the broadcast traffic. The 95 % confidence interval analysis was included to show the accuracy of the simulation results. It would be interesting to compare those findings with other types of AMI deployment.

References

[1] D. Chen, J. Brown, J. Y. Khan, 6lowpan based neighborhood area network for a smart grid communication infrastructure, in: 2013 Fifth International Conference on Ubiquitous and Future Networks (ICUFN), Institute of Electrical & Electronics Engineers (IEEE), 2013. doi:10.1109/icufn.2013.6614885.

[2] D. Chen, J. Brown, J. Y. Khan, Performance analysis of a distributed 6lowpan network for the smart grid applications, in: 2014 IEEE Ninth International Conference on Intelligent Sensors, Sensor Networks and Information Processing (ISSNIP), Institute of Electrical & Electronics Engineers (IEEE), 2014. doi:10.1109/issnip.2014.6827646.

[3] M. Islam, M. M. Uddin, M. A. A. Mamun, M. Kader, Performance analysis of AMI distributed area network using WiMAX technology, in: 2014 9th International Forum on Strategic Technology (IFOST), Institute of Electrical & Electronics Engineers (IEEE), 2014. doi:10.1109/ifost.2014.6991093.

[4] D. Bian, M. Kuzlu, M. Pipattanasomporn, S. Rahman, Analysis of communication schemes for advanced metering infrastructure (AMI), in: 2014 IEEE PES General Meeting | Conference & Exposition, Institute of Electrical & Electronics Engineers (IEEE), 2014. doi:10.1109/pesgm.2014.6939562.

[5] A. Patel, J. Aparicio, N. Tas, M. Loiacono, J. Rosca, Assessing communications technology options for smart grid applications, in: 2011 IEEE International Conference on Smart Grid Communications (SmartGridComm), Institute of Electrical & Electronics Engineers (IEEE), 2011. doi:10.1109/smartgridcomm.2011.6102303.

[6] S. Panchadcharam, G. A. Taylor, Q. Ni, I. Pisica, S. Fateri, Performance evaluation of smart metering infrastructure using simulation tool, in: 2012 47th International Universities Power Engineering Conference (UPEC), Institute of Electrical & Electronics Engineers (IEEE), 2012. doi:10.1109/upec.2012.6398571.

[7] E. B. Rice, A. AlMajali, Mitigating the risk of cyber attack on smart grid systems, Procedia Computer Science 28 (2014) 575–582. doi:10.1016/j.procs.2014.03.070.

[8] M. Yigit, E. A. Yoney, V. C. Gungor, Performance of MAC protocols for wireless sensor networks in harsh smart grid environment, in: 2013 First International Black Sea Conference on Communications and Networking (BlackSeaCom), Institute of Electrical & Electronics Engineers (IEEE), 2013. doi:10.1109/blackseacom.2013.6623380.

[9] F. Aalamifar, L. Lampe, S. Bavarian, E. Crozier, WiMAX technology in smart distribution networks: Architecture, modeling, and applications, in: 2014 IEEE PES T&D Conference and Exposition, Institute of Electrical & Electronics Engineers (IEEE), 2014. doi:10.1109/tdc.2014.6863432.

[10] S. Elyengui, R. Bouhouchi, T. Ezzedine, A comparative performance study of the routing protocols RPL, LOADng and LOADng-CTP with bidirectional traffic for AMI scenario doi:10.1109/iccp.2015.7312719.

[11] E. Ancillotti, R. Bruno, M. Conti, The role of the RPL routing protocol for smart grid communications, IEEE Commun. Mag. 51 (1) (2013) 75–83. doi:10.1109/mcom.2013.6400442.

[12] S. Gormus, F. Tosato, Z. Fan, Z. Bocus, P. Kulkarni, Opportunistic RPL for reliable AMI mesh networks, Wireless Networks 20 (8) (2014) 2147–2164. doi:10.1007/s11276-014-0730-1.

[13] G. Iyer, P. Agrawal, E. Monnerie, R. S. Cardozo, Performance analysis of wireless mesh routing protocols for smart utility networks, in: 2011 IEEE International Conference on Smart Grid Communications (SmartGridComm), Institute of Electrical & Electronics Engineers (IEEE), 2011. doi:10.1109/smartgridcomm.2011.6102301.

[14] G. Iyer, P. Agrawal, R. S. Cardozo, Performance comparison of routing protocols over smart utility networks: A simulation study, in: 2013 IEEE Globecom Workshops, Institute of Electrical & Electronics Engineers (IEEE), 2013. doi:10.1109/glocomw.2013.6825116.

[15] B. Lichtensteig, B. Bjelajac, C. Mueller, C. Wietfeld, RF mesh systems for smart metering: System architecture and performance, in: 2010 First IEEE International Conference on Smart Grid Communications, Institute of Electrical & Electronics Engineers (IEEE), 2010. doi:10.1109/smartgrid.2010.5622071.

[16] C. C. Robusto, The cosine-haversine formula, The American Mathematical Monthly 64 (1) (1957) 38. doi:10.2307/2309088.

[17] X. Chen, Z. Dai, W. Li, H. Shi, A layer-based routing protocol for heterogeneous wireless sensor networks, in: 2012 IEEE International Conference on Communications (ICC), Institute of Electrical & Electronics Engineers (IEEE), 2012. doi:10.1109/icc.2012.6363670.

[18] Hydro-Québec, Remote meter-reading project phase 1, online, http://publicsde.regie-energie.qc.ca/projets/34/DocPrj/R-3770-2011-B-0157-TRAD-DOC-2012_05_23.pdf (May 2012).

[19] F. Malandra, B. Sanso, Analytical performance analysis of a large-scale RF-mesh smart meter communication system, in: 2015 IEEE Power & Energy Society Innovative Smart Grid Technologies Conference (ISGT), Institute of Electrical & Electronics Engineers (IEEE), 2015. doi:10.1109/isgt.2015.7131840.

[20] F. Malandra, B. Sanso, PeRF-mesh: A performance analysis tool for large scale RF-mesh-based smart meter networks with FHSS, in: 2015 IEEE International Conference on Smart Grid Communications (SmartGridComm), Institute of Electrical & Electronics Engineers (IEEE), 2015. doi:10.1109/smartgridcomm.2015.7436398.

[21] Ville de Montréal, Portail Données Ouvertes. List of residential addresses in the island of Montréal. http://donnees.ville.montreal.qc.ca/dataset/adresses-ponctuelles.